Vertical-Substrate MPCVD Epitaxial Nano-diamond Growth

Yan-Kai Tzeng[1], Jingyuan Linda Zhang[2], Haiyu Lu[1,3], Hitoshi Ishiwata[3,4], Jeremy Dahl[3,4], Robert M. K. Carlson[3,4], Hao Yan[3,4], Peter R. Schreiner[5], Jelena Vuckovic[2], Zhi-Xun Shen[1,3,4], Nicholas Melosh[,3,4], Steven Chu[*,1,6]*

[1]Department of Physics, Stanford University, Stanford, California 94305, United States

[2]E. L. Ginzton Laboratory, Stanford University, Stanford, California 94305, United States

[3]Geballe Laboratory for Advanced Materials, Stanford University, Stanford, California 94305, United States

[4]Stanford Institute for Materials and Energy Science, SLAC National Accelerator Laboratory, 257S Sand Hill Road, Menlo Park, California 94025, United States

[5]Institute of Organic Chemistry, Justus-Liebig University, Heinrich-Buff-Ring 17, 35392 Giessen, Germany

[6]Department of Molecular and Cellular Physiology, Stanford University, Stanford, California 94305, United States

ABSTRACT

Color center-containing nanodiamonds have many applications in quantum technologies and biology. Diamondoids, molecular-sized diamonds have been used as seeds in Chemical Vapor Deposition (CVD) growth. However, optimizing growth conditions to produce high crystal quality nanodiamonds with color centers requires varying growth conditions that often leads to ad-hoc and time-consuming, one-at-a-time testing of reaction conditions. In order to rapidly explore parameter space, we developed a microwave plasma CVD technique using a vertical, rather than horizontally oriented stage-substrate geometry. With this configuration, temperature, plasma density and atomic hydrogen density vary continuously along the vertical axis of the substrate. This variation allowed rapid identification of growth parameters that yield single crystal diamonds down to 10 nm in size, and 75 nm diameter optically active centers Silicon-Vacancy (Si-V) nanoparticles. Furthermore, this method may provide a means of incorporating a wide variety of dopants in nanodiamonds without ion irradiation damage.

KEYWORDS: MPCVD, nanodiamond, single-crystal diamond, Si-V center, Cr-related center

TABLE OF CONTENT GRAPHIC

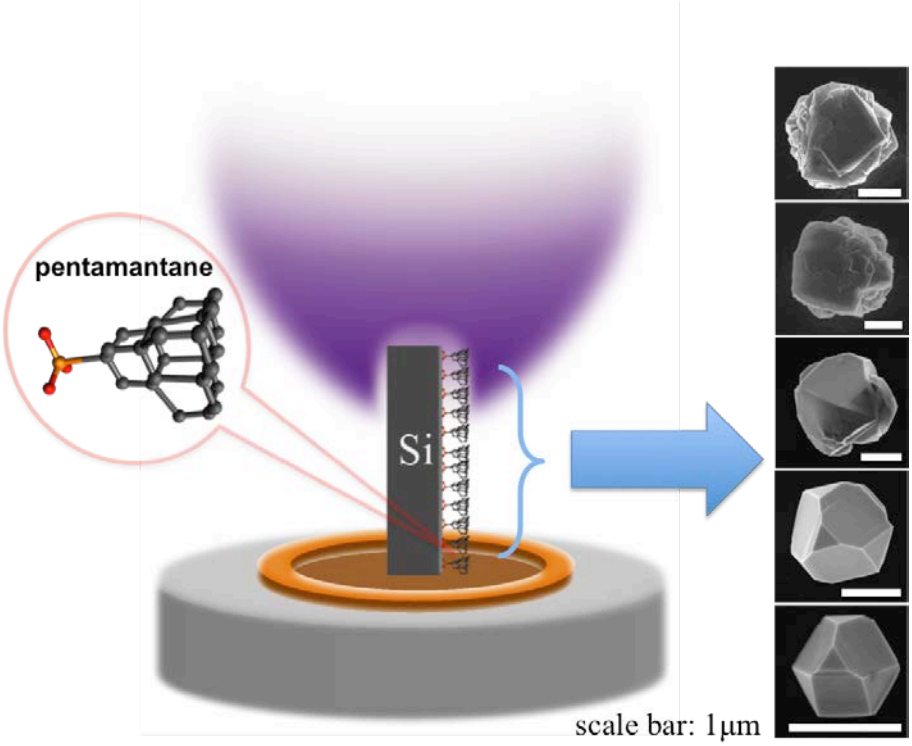

TEXT

Historically, diamond, an sp^3 carbon allotrope, has attracted enormous scientific interest due to its extreme physical, mechanical, optical, and electronic properties. Diamond is currently synthesized under high-pressure-high-temperature (HPHT) conditions[1] or it can be grown directly from diamond seeds at less extreme conditions by chemical vapor deposition (CVD).[2] Driven by breakthroughs in quantum computing,[3] quantum entanglement[4] and encryption,[5] and biolabeling,[6] the controlled synthesis of high-purity diamonds containing color centers has become an important research topic with the promise of a variety of new applications.[7, 8]

Of particular interest, especially for biolabeling, is the incorporation of color centers into nanodiamond due to the fact that diamond is biocompatible, nontoxic, and chemically inert. Two of the most promising types of diamond color centers are nitrogen-vacancy (N-V)[9] and silicon-vacancy (Si-V)[10] centers. These centers can serve as highly photostable and ultra-bright nano-probes for studying cell migration in mice[11] and other applications of super-resolution imaging.[12] Pertsinidis, *et al.*[13] have shown that sub-nanometer spatial resolution is possible if greater than 10^6 signal photons per second can be detected, and it has been found that photostable Si-V color centers can emit up to 5×10^6 counts per second.[10]

In addition, N-V and Si-V centers have demonstrated their potential for quantum information processing and quantum sensing applications.[10, 14] Shallow N-V centers in diamond formed through a sequence of surface treatments can have long spin coherence, and act as high-sensitivity sensors for nuclear magnetic resonance spectroscopy.[15] Microwave and optical methods can control qubit states in N-V centers,[16] facilitating

quantum network,[17] quantum memory,[18] and quantum sensing applications.[14] Si-V centers are also stable, bright, single-photon sources[10] with small inhomogeneous broadening and a large Debye-Waller factor, which are favorable for applications that utilize emitter and photon coherence. Other less common color centers, such as nickel (Ni),[19] chromium (Cr),[20] germanium (Ge),[21] or europium (Eu)[22] have the promise to open up even more avenues of research and applications. For example, nickel-related centers in diamond are particularly interesting due to their electron paramagnetic resonance (EPR).[19] Therefore, developing methodologies to improve the incorporation and control of color centers in diamond is an important research area addressed here.

One common and inexpensive approach for obtaining very small diamonds containing N-V centers is via detonation synthesis, resulting in 5~20 nm "detonation diamonds".[23] The elemental carbon and nitrogen precursors are contained within the explosive itself, e.g. TNT (trinitrotoluene). Unfortunately, due to the uncontrolled nature of the synthesis, incorporation of unwanted sp^2 carbon into the detonation diamonds remains problematic.[24]

Other methods for obtaining color-centers containing nano-diamonds include ball-milling,[25] sonication of polycrystalline nanodiamond thin film,[26] crushing larger diamonds,[27] or subsequent etching bulk diamond.[28] The disadvantage of some of these methods is that they result in highly polydisperse sizes, crystal defects due to the extruding pressure, and increased sp^2 content due to surface graphitization. Some of these drawbacks can be improved through acid treatment, etching, and a sequence of annealing at high temperatures.[29, 30]

A third method that circumvents the shortcomings described above is direct growth of

nanometer-size diamonds using chemical vapor deposition (CVD). CVD offers the potential to grow high-quality, stress-free single-crystal diamonds while introducing color centers during growth through controlled addition of dopants, e.g. nitrogen, silicon, nickel or chromium into the plasma. Challenges facing CVD growth have to do with the size and quality of the diamond seed crystals. If the goal is to grow perfect diamond crystals on the order of several nanometers, very small, very pure, and preferentially very homogeneous seeds are needed. Until recently, such seeds did not exist.

To even attempt to grow high-quality, nanometer-size diamonds, a seed of molecular-size with diamond-structure is required. This rules out all of the more common seeding techniques. Diamondoids can be thought of as hydrogen-terminated diamonds in the 0.5 to 1.0nm size range. As discussed in recent work by Zhang and Ishiwata et al.[31,32] the relatively large ("higher") diamondoids [1(2,3)4] pentamantane, a diamondoid consisting 5 interlocking diamond cages arranged to form a tetrahedron,[33,34] has been shown to be an effective seed. The crystal quality and yield of different diamondoid seeds and also different nanoseeds is the subject of current studies.

Although it was previously shown that CVD diamonds can be grown from pentamantane,[31,32] the methodology was far from optimized. The combined variables of substrate temperature, plasma concentrations, and etching rate of MPCVD growth leads to a very large possible parameter space over which to optimize. To explore a much greater range of conditions, we developed a novel substrate arrangement for CVD growth in which the substrate is rotated 90^{o} from the conventional setup. In this configuration, the substrate and seeds are exposed to systematic variations in plasma density, local temperature, and different growth conditions that help rapidly identify optimal growth

conditions. In addition to providing a means for high-purity nano-diamond growth, the methodology described here provides a simple and reproducible approach for introduction of color centers including Si-V, and Cr-doped nano-diamonds by introducing the dopant impurities into the plasma during growth.

Experiment and Results

A self-assembled monolayer of [1(2,3)4] pentamantane diamondoids was chemically bound to oxidized surfaces of N-type <100> silicon wafers via the reaction of 7-dichlorophosphoryl[1(2,3)4]-pentamantane with the surface oxygen atoms to form strong phosphonate linkages according to a previously described method.[34] Diamond was grown in a microware-plasma CVD (MPCVD, Seki Diamond Systems SDS 5010) with H_2: 300 sccm, CH_4: 0.5 sccm, stage temperature: 350 °C, microwave power: 400 W, pressure: 23 Torr. For optical characterization, diamond growth on the vertically oriented N-typed (Nitrogen-doped) Silicon Carbide <0001> (Thickness: 330 ± 25 μm, Resistivity: 0.02 ~ 0.2 Ω•cm) substrate was optimized at H_2: 300 sccm, CH_4 with 1% SiH_4: 0.5 sccm, stage temperature: 300 °C, microwave power: 300 W, pressure: 23 Torr. To maintain the substrate in a vertical position, we stood the wafer with diamondoid perpendicularly on a molybdenum substrate holder by the two Si-wafers on both sides.

The silicon wafer's vertical orientation yielded a wide range of growth conditions resulting in higher-quality diamonds with better seeding density than using a horizontal substrate (Fig 1). The MPCVD was operated at low stage temperatures (350 °C) and low plasma intensity (400 W), with the top-edge of the silicon wafer (8 mm high, 6 mm wide,

and 0.5 mm thick) acting as a plasma antenna. It is important that the substrate is at least semiconducting, as insulating materials fail to act as an antenna and the advantage of the vertical growth method is lost.

These varied conditions are in contrast with conventional direct plasma CVD diamond growth condition where the stage temperature is typically greater than 850 °C and microwave power greater than 1.3 kW. Such conditions were found to be too harsh for optimal diamond growth from pentamantane seeds. The vertical geometry generates a temperature and plasma electron density gradient along the substrate, allowing the seeds to be exposed to different conditions from top to bottom of the wafer. In addition, simulations described below show that the concentration of atomic hydrogen in the plasma also changes along the length of the vertical substrate.

Representative scanning electron microscope (SEM) images of diamond growth along the length of the wafer show a systematic trend in crystal morphology and diamond particle density. The results of SEM images in Figure 2a show that the diamond particles are more numerous but polycrystalline near the top of the wafer, evolving into well-faceted, single-crystal particles near the bottom of the silicon substrate. The seeding density along the vertical axis and across the width of the substrate was roughly consistent, ~800±100 diamond particles per mm^2, though under certain conditions higher seeding densities were possible (Supplement information Figure S1). Diamond quality was assessed through Raman spectroscopy. As shown in Figure 2b, the Raman spectra of sp^3 (diamond) and sp^2 (graphitic) hybridized carbons are quite distinct. It is important to keep in mind when looking at the Raman spectra that the molar intensity coefficient for the sp^3 vibration is 50x weaker than sp^2 features.[35]

The highest quality diamond nanoparticles occurred 2-3 mm from the bottom of the wafer (Figure 2a), and showed single crystal faceting and a very sharp 1332 cm^{-1} sp^3 Raman peak with the FWHM (Full Width at Half Maximum) line-width of 5.75 cm^{-1} (Red spectra of Figure 2b, 2 mm from the bottom of the substrate). A relatively large fraction (37%) of the diamonds at this location were of high-quality, with faceted crystal morphologies and a sharp sp^3 Raman peak (N = 35, Supplement Information Figure S2 - S4). The mean line-widths of these nanoparticles was 5.60 ± 1.04 cm^{-1}, similar to thin-film diamond[26] and significantly less than most nanoparticles. The narrowest line-widths observed were 3.51 cm^{-1}, remarkably close to the 3.0 cm^{-1} line-width typically seen in bulk diamond[36] (Figure 2e). Interestingly, polycrystalline particles or those with visible defects had higher linewidths than similarly sized, faceted single crystals, suggesting crystalline defects were at least partially responsible for linewidth broadening. For comparison, a collection of the SEM images and Raman sp^3 peaks for all 35 nanoparticles analyzed are shown in Supplement Information.

A bright-field transmission electron microscope (TEM) image taken on a single crystal silicon TEM grid and the Fourier transform of the lattice image of a 10 nm diameter nanodiamond are shown in Figure 3a, b. The distance between the two neighboring planes is 0.206 nm, corresponding to the diamond {111} lattice. An image of the electron diffraction ring pattern (Figure 3c) and FFT (Fast Fourier Transform) lattice spacing (Figure 3b) is consistent with a dislocation-free, high-quality diamond nanocrystals.

These results show that the largest but least pure (i.e. most sp^2 contamination) diamonds and diamond-like nanoparticles were found to grow on the top of the wafer

(figure 2a). Towards the bottom (away from the plasma), smaller, higher-quality, pure sp^3 diamonds grew. We believe that this phenomenon is the result of higher concentrations of atomic hydrogen acting as an sp^2 etchant near the bottom of the wafer. This hypothesis is supported by the numerical simulations described below. These results show that using this growth geometry, one can continuously screen a variety growth conditions, e.g. plasma electron density, atomic hydrogen density, temperature and gas composition, to better optimize high seeding densities, crystal quality, and the incorporation of desired dopants.

Computer simulations

To understand the different growth environments present as a function of distance along the wafer for vertical CVD diamond growth, we performed a series of computer simulations of the growth conditions. Our simulations of the vertical-substrate MPCVD were performed using the commercial software Comsol Multiphysics. In the model, electromagnetic radiation creates hot electrons, which in turn heat up the neutral gas via rotational and vibrational excitations.[37–39] For our plasma model, we used Maxwell's equations for electromagnetic field in combination with a drift-diffusion equation (Supplementary Information, Eq. 1) for electrons and the modified Maxwell-Stefan equation (Supplementary Information, Eq. 2) for the transport of neutrals and ions. To improve the simulations, both Navier-Stokes and heat transfer equations were included to determine the plasma temperature and gas flow rate. Atomic hydrogen created by electron-impact dissociation of H_2 is the driving force behind all the reactions. The atomic hydrogen in the plasma plays a vital role during the growth of diamond MPCVD

since it suppresses the formation of graphite and stabilizes diamond growth.[40]

Simulations included the collisions of seven electron-neutrals or the three ions listed in table S1 (Supplementary Information). At our operating pressure of 23 Torr, the mean free path of neutral gas collisions is ~600 μm, much shorter than the internal dimensions of the CVD chamber. Hence, energetic neutral atoms heat the surrounding gas molecules before colliding with the chamber walls. Through the dissociation and ionization processes, the accelerated electrons are also capable of generating radical neutrals and ions.

Modeling results suggest that the plasma electron density is concentrated on the top-edge of a vertically placed Si-wafer, consistent with visual emission observations (Figure 4b). The vertical substrate creates a gradient of ionic methane and hydrogen over the length of the wafer. The atomic hydrogen concentration and temperature gradients along the z-axis at a microwave power of 400 W is presented in Figure 4c. Near the top of silicon wafer, the temperature is higher (~950ºC), with a lower density of atomic hydrogen. Conversely, near the bottom of the wafer where optimal crystal faceting and quality is observed, the atomic hydrogen concentration is higher, with a lower substrate temperature (~600ºC). We believe the higher atomic hydrogen concentration with concomitant higher carbon etch rates leads to the higher quality nanodiamond in the lower portion of the wafer.

In order to test the predictions of the temperature gradient between simulation and experiment, we used the infrared pyrometer (LumaSense Technologies Inc, USA) to acquire temperatures along the height of the vertical substrate. The resulting measurements, which are shown in Figure 4d, indicate an increase in temperature from

550ºC at 2 mm to 750ºC at 5 mm, commensurate with the simulations. As was shown in our results, atomic hydrogen etching and plasma density during growth plays a crucial role in the final quality of the epitaxial single-crystal nanodiamond. Moreover, the etching allows the removal of any non-epitaxial carbon atom, thus leading to better morphology of grown nanodiamonds.

Optical Characterization of Color Centers

The Si and N dopants were incorporated during the CVD plasma growth process. These elements could be introduced either through addition of reagent gases (N_2 or SiH_4)[41], or through etching of a Si substrate during vertical CVD growth. Thus, using silicon or silicon carbide (SiC) substrates during the CVD process resulted in the growth of diamonds with Si-V color centers without additional Si sources in the feed gas.

An important aspect of the color center behavior is correlating nanodiamond size and morphology to optical properties. After growth, a fiducial mark was made ~2mm from the base of the wafer to facilitate one-to-one comparison between confocal fluorescence imaging and SEM. This enabled correlation of the SEM imaging showing diamonds size and quality with fluorescence, as shown by the inset of Figure 5c. Optical characterization of the color centers was performed using a scanning confocal microscope coupled to a spectrometer (Supplementary Information, Figure S6). When examining diamonds with Si-V centers grown on Si wafers, we observed that photo-quenching from the Si substrate greatly limited photoluminescence intensity. To reduce this problem, we grew the nanodiamonds on nitrogen-doped 6H-SiC, which has lower background emission (Supplementary Information, Figure S5) and less quenching than

that of silicon substrate due to its larger band gap.

Representative results of confocal photoluminescence and SEM imaging of three diamond nanoparticles are shown in Figure 5a and Figure 5b, respectively. Si-V centers in nanodiamonds with low crystal strain and cryogenic temperatures (<40K) should exhibit four zero phonon lines (ZPLs). At 4.5 K, we found that the photoluminescence spectra of a 75 nm diameter single-crystal nanodiamond shows more than four transitions, indicating that more than one color center could be incorporated in these small nanodiamonds (Figure 5c). The lifetime of these Si-V color centers (ND 1) is about 0.602±0.008 ns as shown in Figure 5d. This result is close to the literature value of 0.7 ~ 1.2 ns.[10]

This synthetic method was applicable to other color centers as well. For example, it was also possible to incorporate chromium color centers during the CVD process (Supplementary Information, Figure S8). Previously, optically active Cr-related centers could be produced by co-implantation[42] with O, N, or Si, and could have similar brightness and radiative lifetimes as Si-V centers.[43] Here, a solution of $[Cr(H_2O)_6](NO_3)_3$ was simply dried onto the Si substrate, then placed into the microwave growth chamber and grown under the same conditions as SiV synthesis. Nanoparticles produced via this process showed clear optical signatures of Cr centers, with photoluminescence peaks at 750 nm and 758 nm (Supplementary Information). This process did not require a second impurity atom (i.e. O, N, or Si), suggesting vertical-substrate MPCVD could be a general means of creating a wide variety of color centers, e.g. the rare earth elements related centers.

Conclusion

Recent advancements in the fields of quantum computing, bio-sensing, quantum entanglement and encryption, have created the need for the development of improved methods for obtaining very small, very high-quality diamonds containing color centers. Using pentamantane diamondoids chemically attached to a substrate as seeds and a novel plasma/substrate geometry in which the substrate is rotated by 90^{o}, we have been able to grow very high quality single-crystal diamonds in the 10 nm size range, and Si-V center-containing diamonds in the ~75 nm size range. Based on these results this technique may be a viable means for incorporating a wide variety of possible dopants into small diamonds to create color centers including Ge-V, Ni-related, and rare earth elements. Furthermore, because vertical substrate diamond growth explores a wide variety of temperatures and plasma compositions, it is an excellent technique to study fundamental aspects of CVD diamond growth.

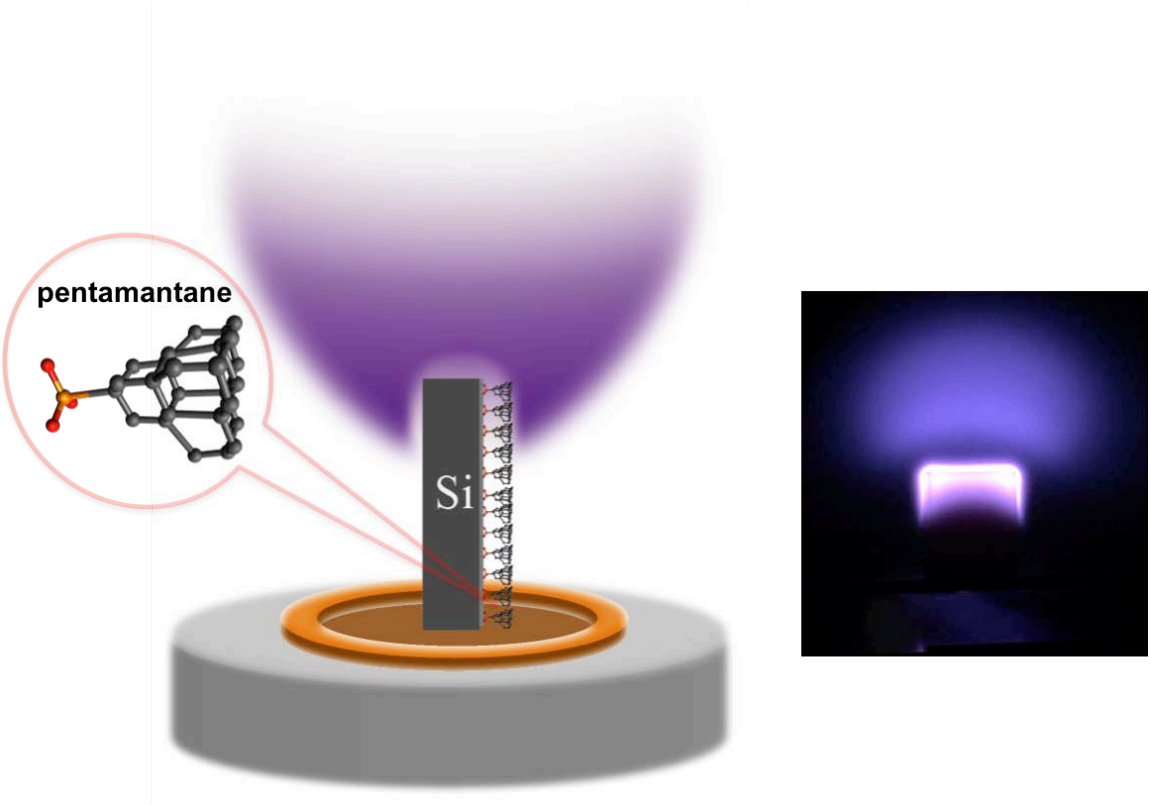

Figure 1: Schematic illustration and a photo of the vertical-substrate MPCVD diamond growth. [1(2,3)4]Pentamantane was chemically bonded to oxidized surfaces of silicon wafers via phosphonyl dichloride and then rotated the substrate is rotated 90° to a vertical configuration for MPCVD diamond growth. The hydrogen plasma is concentrated on the top edge, as shown in figure.

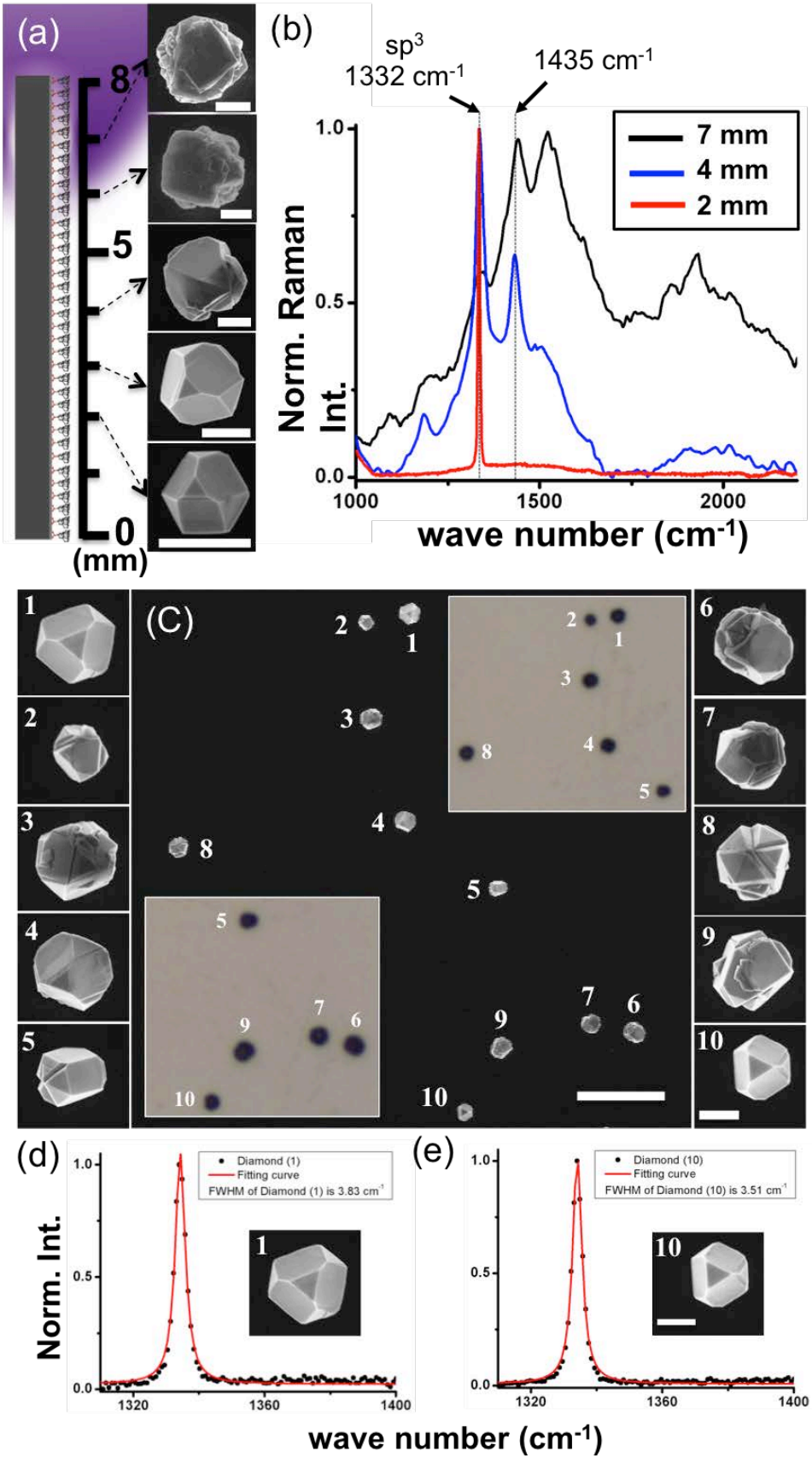
(a)
8
5
0
(mm)
(b)
sp3
1332 cm-1
1435 cm-1
7 mm
4 mm
2 mm
Norm. Raman Int.
1.0
0.5
0.0
1000
1500
2000
wave number (cm-1)
(C)
(d)
Diamond (1)
Fitting curve
FWHM of Diamond (1) is 3.83 cm-1
Norm. Int.
(e)
Diamond (10)
Fitting curve
FWHM of Diamond (10) is 3.51 cm-1
1320
1360
1400
wave number (cm-1)

Figure 2: Characteristics of diamond crystal at different height of the substrate (Si-wafer). (a) The morphology of diamonds was changed along the different height of Si-wafer substrate, scale bar: 1μm. (b) Raman spectra of diamond samples from different substrate heights. The diamond peak of sp^3 is at 1332 cm^{-1} and the linewidth of Raman FWHM is 5.75 cm^{-1} at the height of 2 mm. The Raman peak of 1435 cm^{-1} is most likely transpolyacetylene.[44] (c) SEM imaging map of diamond at the height of ~2 mm was on silicon substrate, scale bar: 10 μm. Each diamond image is shown on both sides, scale bar: 1 μm. The bottom region (at the height of 2 mm) produces around 20 ~ 30 % high-quality, single crystal diamond with a narrow-line sp^3 Raman peak. [Inserted pictures were the correlated wide-field imaging from confocal Raman spectroscopy.] (d)(e) Raman spectra of diamond (1) and (10) have the FWHM of sp^3 Raman peaks, 3.81 cm^{-1} and 3.51 cm^{-1} separately. Other results of diamond particles are shown in the Supplement Information. Following condition: total gas pressure, microwave power, flow rate of hydrogen gas, flow rate of methane, stage temperature, and growth time were, respectively, 23 Torr, 350 W, 300 sccm, 0.5 sccm, 350 °C, and 4hrs.

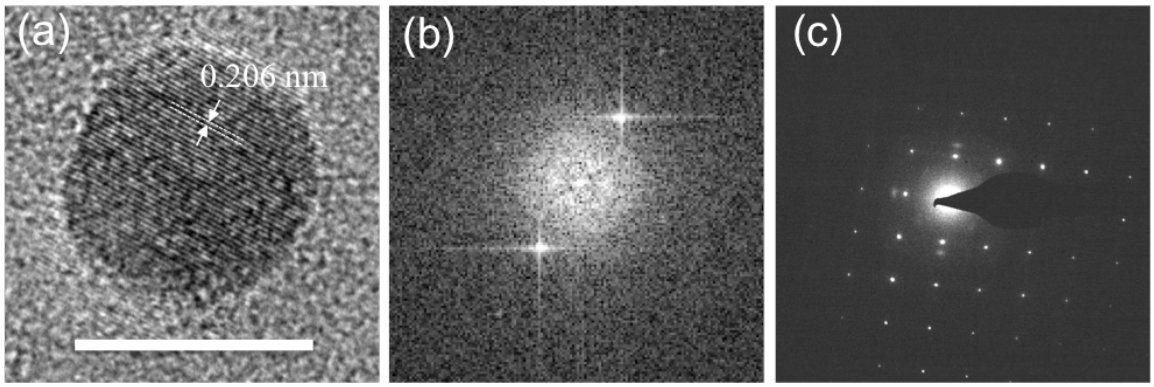

Figure 3: TEM, FFT and SAED images of diamond nanocrystals. (a) Bright-field TEM (transmission electron microscopy) image, Scale bar: 10nm, (b) the corresponding FFT (Fast Fourier Transform) image (c) the image of selected area electron diffraction (SAED) patterns. Following condition: total gas pressure, microwave power, flow rate of hydrogen gas, flow rate of methane, stage temperature, and growth time were, respectively, 23 Torr, 400 W, 300 sccm, 0.5 sccm, 350 °C, and 20 mins.

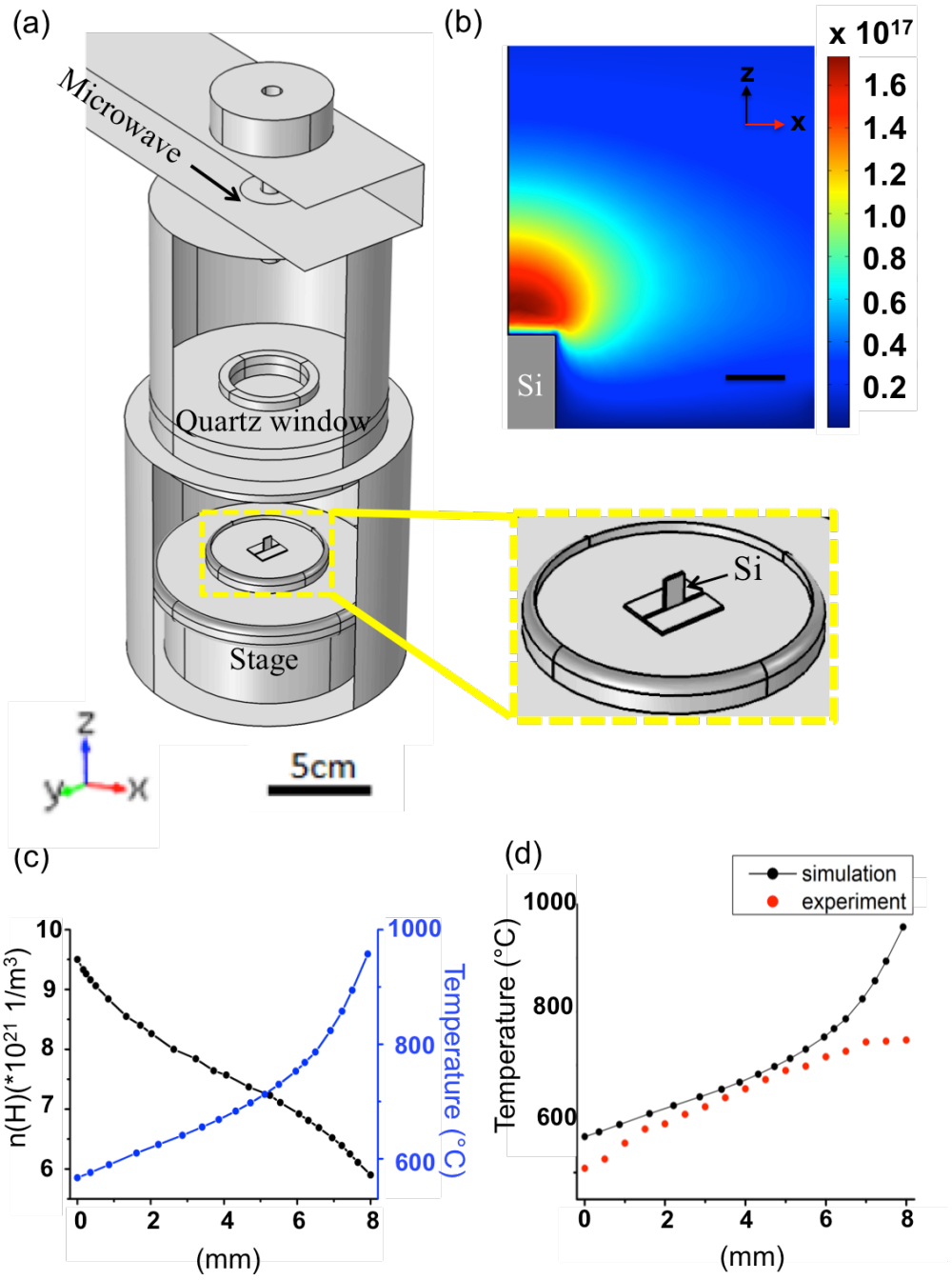

Figure 4: Simulation results of vertical-substrate MPCVD. (a) Simulation model, the semi-conductive substrate size is 8 mm in height, 6 mm in width. (b) Distribution of plasma electron density. Scale bar: 5 mm. (c) From bottom (0 mm) to top (8 mm), simulation results show the temperature gradient of substrate and the distribution of atomic hydrogen. (d) Comparison between experimental and simulated temperatures along the vertical axis.

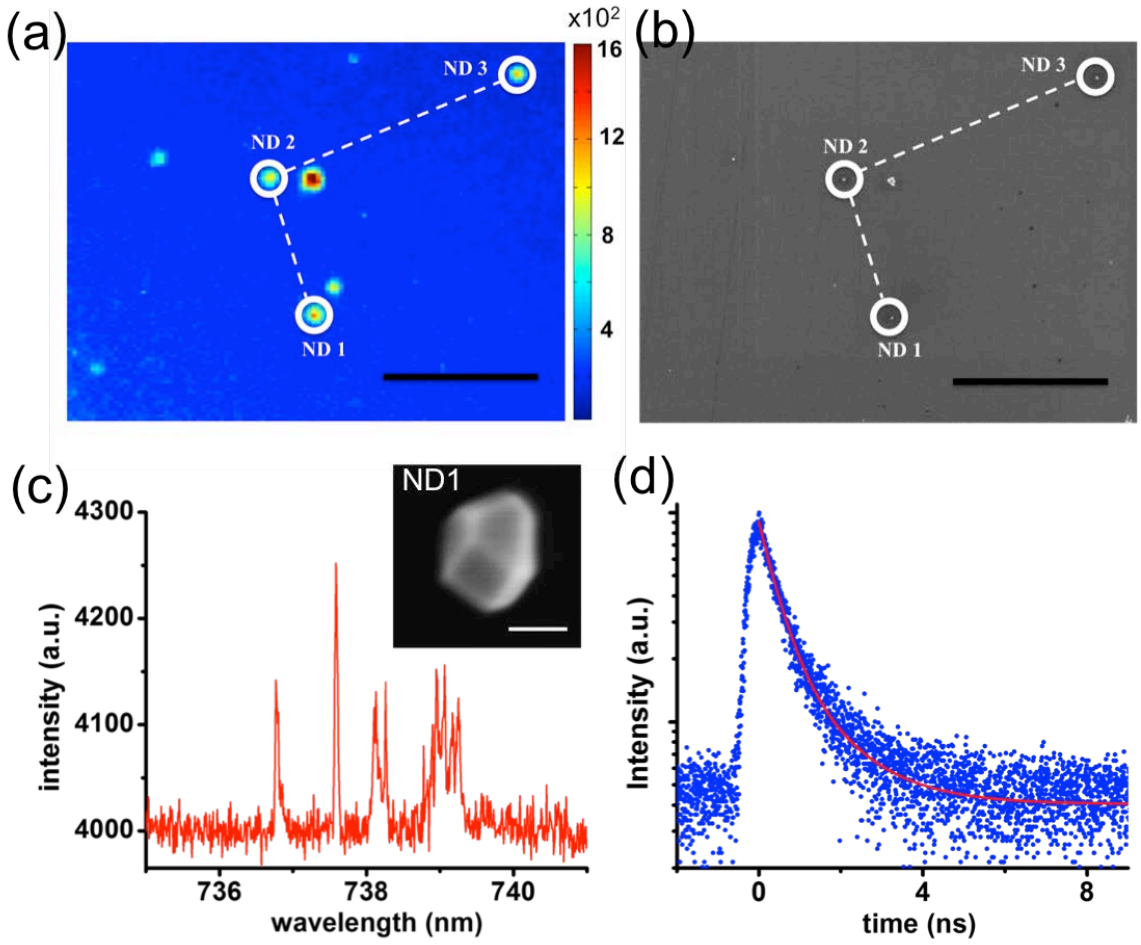

Figure 5: Optical characterization of SiV color centers in nanodiamonds grown by vertical-substrate MPCVD. (a) Scanning confocal photoluminescence map of nanodiamonds containing SiV on a silicon carbide substrate (Nitrogen-doped 6H-SiC), correlating with the (b) SEM image of the same region. Scale bar: 10 μm. (c) High-resolution photoluminescence spectrum of the fine structure lines of SiV color center in ND 1 at 4.5 K; the multiple peaks indicate several color centers in this particle. Inset is SEM image of ND 1 under high magnification, with the single crystal facets clearly showing. Scale bar: 50 nm. (d) Time resolved photoluminescence of ND1 indicates a lifetime of 0.602±0.008 ns at room temperature, implying substrate quenching on some of the photoluminescence. The photoluminescence spectra and SEM images of both ND2 and ND3 are shown in Supplementary Information Figure S7. The sample is grown under the following condition: total gas pressure: 23 Torr; microwave power: 300 W; flow rate

of hydrogen gas: 300 sccm; flow rate of methane: 0.5 sccm; stage temperature: 330 °C; and growth time: 15 mins.

ASSOCIATED CONTENT

Supporting Information

Details on the simulation, optical setup and characterization, substrate measurement, and Cr-related center of sample preparation and results are supplied in the Supporting Information.

AUTHOR INFORMATION

Corresponding Authors

* E-mail: Nicholas Melosh: nmelosh@stanford.edu; Steven Chu: schu@stanford.edu

Present Addresses

Hitoshi Ishiwata's present address: Department of Physical Electronics, Tokyo Institute of Technology, 2-12-1 Ookaya-ma, Meguro-ku, Tokyo 152-8552, Japan.

Author Contributions

The manuscript was written through contributions of all authors. All authors have given approval to the final version of the manuscript.

ACKNOWLEDGEMENT

This work is supported by the Department of Energy, Laboratory Directed Research and Development program at SLAC National Accelerator Laboratory, under contract DE-AC02-76SF00515, and a grant No. 4309 from the Moore Foundation.

Notes

The authors declare no competing financial interest.

REFERENCES

(1) Boudou, J. P.; Tisler, J.; Reuter, R.; Thorel, A.; Curmi, P. a.; Jelezko, F.; Wrachtrup, J. *Diam. Relat. Mater.* **2013**, *37*, 80–86.

(2) Butler, J. E.; Sumant, A. V. *Chem. Vap. Depos.* **2008**, *14* (7–8 SPEC. ISS.), 145–160.

(3) Wrachtrup, J.; Jelezko, F. *J. Phys. Condens. Matter* **2006**, *18* (21), S807–S824.

(4) Hensen, B.; Bernien, H.; Dréau, a. E.; Reiserer, a.; Kalb, N.; Blok, M. S.; Ruitenberg, J.; Vermeulen, R. F. L.; Schouten, R. N.; Abellán, C.; Amaya, W.; Pruneri, V.; Mitchell, M. W.; Markham, M.; Twitchen, D. J.; Elkouss, D.; Wehner, S.; Taminiau, T. H.; Hanson, R. *Nature* **2015**, *526* (7575), 682–686.

(5) Hirose, M.; Cappellaro, P. *Nature* **2016**, *532* (7597), 77–80.

(6) Chang, B. M.; Lin, H. H.; Su, L. J.; Lin, W. Der; Lin, R. J.; Tzeng, Y. K.; Lee, R. T.; Lee, Y. C.; Yu, A. L.; Chang, H. C. *Adv. Funct. Mater.* **2013**, *23* (46), 5737–5745.

(7) Balasubramanian, G.; Chan, I. Y.; Kolesov, R.; Al-Hmoud, M.; Tisler, J.; Shin, C.; Kim, C.; Wojcik, A.; Hemmer, P. R.; Krueger, A.; Hanke, T.; Leitenstorfer, A.; Bratschitsch, R.; Jelezko, F.; Wrachtrup, J. *Nature* **2008**, *455* (7213), 648–651.

(8) Staudacher, T.; Shi, F.; Pezzagna, S.; Meijer, J.; Du, J.; Meriles, C. a; Reinhard, F.; Wrachtrup, J. *Science* **2013**, *339* (6119), 561–563.

(9) Gruber, a.; Dräbenstedt, A.; Tietz, C.; Fleury, L.; Wrachtrup, J.; Borczyskowski, C. Von. *Science (80-.).* **1997**, *276* (5321), 2012–2014.

(10) Neu, E.; Steinmetz, D.; Riedrich-Möller, J.; Gsell, S.; Fischer, M.; Schreck, M.; Becher, C. *New J. Phys.* **2011**, *13*, 25012.

(11) Wu, T.-J.; Tzeng, Y.-K.; Chang, W.-W.; Cheng, C.-A.; Kuo, Y.; Chien, C.-H.; Chang, H.-C.; Yu, J. *Nat. Nanotechnol.* **2013**, *8* (9), 682–689.

(12) Tzeng, Y. K.; Faklaris, O.; Chang, B. M.; Kuo, Y.; Hsu, J. H.; Chang, H. C. *Angew. Chemie - Int. Ed.* **2011**, *50* (10), 2262–2265.

(13) Pertsinidis, A.; Zhang, Y.; Chu, S. *Nature* **2010**, *466* (7306), 647–651.

(14) Maze, J. R.; Stanwix, P. L.; Hodges, J. S.; Hong, S.; Taylor, J. M.; Cappellaro, P.; Jiang, L.; Dutt, M. V. G.; Togan, E.; Zibrov, A. S.; Yacoby, A.; Walsworth, R. L.; Lukin, M. D. *Nature* **2008**, *455* (7213), 644–647.

(15) Lovchinsky, I.; Sushkov, A. O.; Urbach, E.; de Leon, N. P.; Choi, S.; De Greve, K.; Evans, R.; Gertner, R.; Bersin, E.; Müller, C.; McGuinness, L.; Jelezko, F.; Walsworth, R. L.; Park, H.; Lukin, M. D. *Science* **2016**, *351* (6275), 836–841.

(16) Yale, C. G.; Buckley, B. B.; Christle, D. J.; Burkard, G.; Heremans, F. J.; Bassett, L. C.; Awschalom, D. D. *Proc. Natl. Acad. Sci.* **2013**, *110* (19), 7595–7600.

(17) Bernien, H.; Hensen, B.; Pfaff, W.; Koolstra, G.; Blok, M. S.; Robledo, L.; Taminiau, T. H.; Markham, M.; Twitchen, D. J.; Childress, L.; Hanson, R. *Nature* **2013**, *497* (7447), 86–90.

(18) Maurer, P. C.; Kucsko, G.; Latta, C.; Jiang, L.; Yao, N. Y.; Bennett, S. D.; Pastawski, F.; Hunger, D.; Chisholm, N.; Markham, M.; Twitchen, D. J.; Cirac, J. I.; Lukin, M. D. *Science (80-.).* **2012**, *336* (6086), 1283–1286.

(19) Loubser, J. H. N.; Ryneveld, W. P. Van. *Nature* **1966**, *211*, 517.

(20) Aharonovich, I.; Castelletto, S.; Simpson, D. a.; Stacey, A.; McCallum, J.; Greentree, A. D.; Prawer, S. *Nano Lett.* **2009**, *9* (9), 3191–3195.

(21) Iwasaki, T.; Ishibashi, F.; Miyamoto, Y.; Doi, Y.; Kobayashi, S.; Miyazaki, T.;

Tahara, K.; Jahnke, K. D.; Rogers, L. J.; Naydenov, B.; Jelezko, F.; Yamasaki, S.; Nagamachi, S.; Inubushi, T.; Mizuochi, N.; Hatano, M. *Sci. Rep.* **2015**, *5*, 12882.

(22) Magyar, A.; Hu, W.; Shanley, T.; Flatté, M. E.; Hu, E.; Aharonovich, I. *Nat. Commun.* **2014**, *5*, 3523.

(23) Mochalin, V. N.; Shenderova, O.; Ho, D.; Gogotsi, Y. *Nat. Nanotechnol.* **2012**, *7* (1), 11–23.

(24) Van Thiel, M.; Ree, F. H. *J. Appl. Phys.* **1987**, *62* (5), 1761–1767.

(25) Boudou, J.-P.; Curmi, P. a.; Jelezko, F.; Wrachtrup, J.; Aubert, P.; Mohamed Sennour; Balasubramanian, G.; Reuter, R.; Thorel, A.; Gaffet, E. *Nanotechnology* **2009**, *20* (23), 235602.

(26) Zhang, H.; Aharonovich, I.; Glenn, D. R.; Schalek, R.; Magyar, A. P.; Lichtman, J. W.; Hu, E. L.; Walsworth, R. L. *Small* **2014**, *10* (10), 1908–1913.

(27) Su, L.-J.; Fang, C.-Y.; Chang, Y.-T.; Chen, K.-M.; Yu, Y.-C.; Hsu, J.-H.; Chang, H.-C. *Nanotechnology* **2013**, *24* (31), 315702.

(28) Andrich, P.; Alemán, B. J.; Lee, J. C.; Ohno, K.; De Las Casas, C. F.; Heremans, F. J.; Hu, E. L.; Awschalom, D. D. *Nano Lett.* **2014**, *14* (9), 4959–4964.

(29) Chu, Y.; Leon, N. De; Shields, B.; Hausmann, B. J. M.; Evans, R.; Burek, M. J.; Markham, M.; Stacey, A.; Zibrov, A.; Twitchen, D.; Loncar, M.; Park, H.; Maletinsky, P.; Lukin, M. D. *Nano Lett.* **2014**, *14*, 1982–1986.

(30) Evans, R. E.; Sipahigil, A.; Sukachev, D. D.; Zibrov, A. S.; Lukin, M. D. *Phys. Rev. Appl.* **2016**, *5* (4), 1–8.

(31) Ishiwata, H. Molecular Diamonds Enabled Synthesis and Growth, Stanford University, 2015.

(32) Zhang, J. L.; Ishiwata, H.; Babinec, T. M.; Radulaski, M.; Müller, K.; Lagoudakis, K. G.; Dory, C.; Dahl, J.; Edgington, R.; Soulière, V.; Ferro, G.; Fokin, A. A.; Schreiner, P. R.; Shen, Z. X.; Melosh, N. A.; Vučković, J. *Nano Lett.* **2016**, *16* (1), 212–217.

(33) Dahl, J. E.; Liu, S. G.; Carlson, R. M. K. *Science* **2003**, *299* (5603), 96–99.

(34) Fokin, A. a.; Yurchenko, R. I.; Tkachenko, B. a.; Fokina, N. a.; Gunawan, M. a.; Poinsot, D.; Dahl, J. E. P.; Carlson, R. M. K.; Serafin, M.; Cattey, H.; Hierso, J. C.; Schreiner, P. R. *J. Org. Chem.* **2014**, *79* (11), 5369–5373.

(35) Tsai, H. *J. Vac. Sci. Technol. A Vacuum, Surfaces, Film.* **1987**, *5* (6), 3287.

(36) Neu, E.; Arend, C.; Gross, E.; Guldner, F.; Hepp, C.; Steinmetz, D.; Zscherpel, E.; Ghodbane, S.; Sternschulte, H.; Steinmüller-Nethl, D.; Liang, Y.; Krueger, A.; Becher, C. *Appl. Phys. Lett.* **2011**, *98* (24), 6–9.

(37) Hsu, W. L. *J. Appl. Phys.* **1992**, *72* (7), 3102.

(38) Frenklach, M.; Wang, H. *Phys. Rev. B* **1991**, *43* (2), 1520–1545.

(39) Alman, D. a.; Ruzic, D. N.; Brooks, J. N. *Phys. Plasmas* **2002**, *9* (2), 738.

(40) Prelas, M. a; Popovici, G.; Bigelow, L. K.; Dekker, M.; Llc, C. R. C. P. **1998**, *1045* (10), 1045–1048.

(41) Vlasov, I. I.; Barnard, A. S.; Ralchenko, V. G.; Lebedev, O. I.; Kanzyuba, M. V.; Saveliev, A. V.; Konov, V. I.; Goovaerts, E. *Adv. Mater.* **2009**, *21* (7), 808–812.

(42) Aharonovich, I.; Castelletto, S.; Johnson, B. C.; McCallum, J. C.; Prawer, S. *New J. Phys.* **2011**, *13*, 45015.

(43) Aharonovich, I.; Castelletto, S.; Simpson, D. A.; Greentree, A. D.; Prawer, S. *Phys. Rev. A - At. Mol. Opt. Phys.* **2010**, *81* (4), 1–7.

(44) Ferrari, A. C.; Robertson, J. *Phys. Rev. B* **2001**, *63* (12), 121405.